Revisiting nonlinear optical trapping of a single nanoparticle using generalized Lorentz-Mie theory

Anita Devi [2,3,*] Bhaswardeep Sikdar [3] and Arijit K. De [1,†]

[1]*Department of Physical Sciences Indian Institute of Science Education and Research (IISER) Mohali, Knowledge City, Sector 81, SAS Nagar, Punjab 140306, India*

[2]*Department of Chemical Sciences, Indian Institute of Science Education and Research (IISER) Mohali, Knowledge City, Sector 81, SAS Nagar, Punjab 140306, India*

[3]*Department of Physics, University of Alberta, 85 Avenue, Edmonton, Alberta, Canada T6G 2R3*

(Received 27 December 2021; accepted 13 May 2022; published 31 May 2022)

The elusive role of femtosecond pulsed excitation in enhancing the efficiency of optical trapping of nanoparticles over continuous-wave excitation is revisited. Using generalized Lorentz-Mie theory, optical trapping force on nanoparticles composed of materials having a wide range of linear refractive indices, including metamaterials having negative refractive indices, is investigated. It is shown how the incorporation of optical nonlinearity, fine-tuned by the laser parameters (for example, average power, pulse width, etc.), leads to the emergence of novel phenomena such as trap splitting facilitating trapping of multiple particles that were not captured in a previous study on nanoparticles with varying refractive indices using dipole approximation. Intriguingly, we show that the trap becomes highly stable due to negative optical scattering force, known as "Fano resonance." Furthermore, we observe the disappearance and reappearance of trapping wells with increasing refractive index under both continuous-wave and pulsed excitations. These findings show promising applications in the field of photonics through nanoscale optical manipulation controlled by optical nonlinearity.

DOI: 10.1103/PhysRevA.105.053529

I. INTRODUCTION

Over the past few decades, a wide range of materials with nanoscale dimensions were synthesized which found broad applications due to their unique properties (for example, electron confinement), leading to the development of the vast field of nanotechnology. The significance of these materials was apparent when researchers discovered that size might affect a substance's chemical and physical properties, including unique optical properties. The manipulation of nanoparticles using optical tweezers (OT) has gained attention due to the ability to apply force directly to nanoparticles [1,2], such as exploring the physics of rheology [3,4], manipulating macromolecules [5] and metallic nanoparticles [6], quantitatively measuring minuscule vital force [7,8], and so on. Ever since the invention of the OT, most researchers have used continuous-wave (cw) excitation for trapping. However, there were a few cases where micro- or nanosecond pulsed excitations were used, which conjectured that pulsed excitation might provide more efficient trapping of nanoparticles. On the other hand, in spite of the wide use of high-repetition-rate pico- or femtosecond pulsed excitation at similar average power, the advantages of using it over cw excitation remain elusive since only a limited number of experiments with femtosecond pulse laser were conducted [9–18]. The noteworthy fact with pulsed excitation is that it has a substantially higher peak intensity that is high enough to ensure a variety of nonlinear optical phenomena. Thus, under pulsed excitation, without including the nonlinear effects, it would be fallacious to determine the real-time dynamics of particles.

In 2016, our group showed the importance of optical nonlinearity in trapping under pulsed excitation for dielectric nanoparticles [19]. We showed that using femtosecond lasers is one of the more promising and theoretically demonstrated ways to increase optical trapping capabilities for low refractive index (RI) nanoparticles [20,21]. Besides, a few other research groups reported that the trap stiffness of a silica particle does not show a substantial change under pulsed excitation [12], even though these results contradicted those on polystyrene particles [18]. We recently observed a significant change in trap stiffness under pulsed excitation compared to cw excitation and provided a detailed explanation of nonlinear phenomena, combining theory and experiment for polystyrene particles [20]. This is because polystyrene's nonlinear RI is higher than silica. The considerable contribution of nonlinear phenomena gives a significant shift in trap stiffness for polystyrene particles [19,20].

These findings prompted us to explore beyond polystyrene nanoparticles, i.e., to investigate the optical trapping of dielectric nanoparticles with varying RIs [21]. Additionally, using generalized Lorentz-Mie theory (GLMT), we showed how optical nonlinearity could lead to split trapping wells accommodating multiple polystyrene nanoparticles [22] that were not captured in earlier studies using dipole approximation [19]. In this paper, we integrate these two concepts and present theoretical studies on the trapping of dielectric nanoparticles with varying RIs using GLMT, eventually including optical nonlinearity under femtosecond pulsed excitation. This study

*adevi@ualberta.ca
†akde@iisermohali.ac.in

also explains why antireflection coatings are required to trap high-RI particles [23,24]. This work compares the trapping efficiency of cw and pulsed excitations. It determines their pros and cons in various regimes depending on the properties of nanoparticles. Interestingly, we observe the disappearance and reappearance of trapping wells under both cw and pulsed excitations. Unique nonlinear optical phenomena such as trap splitting and Fano resonance are also observed to emerge, which helps in trapping and manipulating nanoparticles that cannot be extensively modulated by cw excitation. We also present a detailed discussion of the trapping and manipulating nanoparticles made of metamaterials having negative RIs that have drawn much attention in recent years due to their novel optical properties [25].

II. METHOD

Here, we discuss the trapping force and potential along the axial direction only because the force and potential is harmonic along the radial direction, giving a stable trap. The value of M (relative RI $= \frac{n_0^p}{n_0^w}$; here n_0^w is the RI of the surrounding medium and n_0^p is the RI of the particle) only controls the type of force (attractive or repulsive) [21]. The type of total force in the axial direction cannot be determined just by the value of M because it is contributed by both gradient and scattering forces, which change with M in various ways. Metamaterials is an emerging field because of its unique property of having either negative permeability (ϵ) or permittivity (μ) or both [26]. One of the examples for epsilon negative metamaterials (ENG) is noble metals [26–28], while gyrotropic or gyromagnetic materials have mu-negative metamaterials (MNG) [26,27]. A combination of both materials exhibits distinct properties such as resonances, anomalous tunneling, transparency, etc. Besides, a few metamaterials have both negative permeability and permittivity, resulting in negligible dispersion [29,30]. Therefore, the effect of permittivity dispersion for metamaterials has been ignored near 800 nm for nanoparticles in our simulations. A detailed explanation is given Sec. A in Appendix. Please note that all the simulations are done here for spherical nanoparticles (nonmagnetic and isotropic) using localized approximation within GLMT. The force component along the axial direction on axis is [31]

$$F_{\text{axial}}^{\text{GLMT}}(z;\ r=0) = \left(\frac{n^w}{c}\right)\left(\frac{2P_{\text{peak/average}}}{\pi w_0^2}\right)C_n^{pr}(z), \qquad (1)$$

where $C_n^{pr}(z)$ is the pressure cross section given by [31–33]

$$C_n^{pr}(z) = \left(\frac{\lambda^2}{2\pi}\right)\sum_n\left[\left(\frac{2n+1}{n(n+1)}\right)|g_n|^2 S_n^{(1)} + \left(\frac{n(n+2)}{n+1}\right)\text{Re}\left[g_n g_{n+1}^* S_n^{(2)}\right]\right], \qquad (2)$$

where $S_n^{(1)} = \text{Re}(a_n + b_n - 2a_n b_n^*)$, and $S_n^{(2)} = (a_n + b_n + a_{n+1}^* + b_{n+1}^* - 2a_n a_{n+1}^* - 2b_n b_{n+1}^*)$ are the combination of Mie scattering coefficients (a_n and b_n; MSCs). Earlier work [22] determined that the first term in Eq. (2) (highlighted in gray) corresponds to the scattering force, and the second term corresponds to the gradient force (highlighted in cyan). g_n in Eq. (2) corresponds to the beam shaping coefficients (BSCs). Since we use localized approximation, g_n is approximated corresponding to the standard BSCs [31–33]. BSCs using localized approximation can be expressed as [31–33] $g_n = iQ\exp[-iQ(\frac{\rho_n}{\omega_0})^2]\exp[ikz_0]$. Here, $Q = \frac{1}{i+2\frac{z-z_0}{l}}$, $l = k\omega_0^2$ is the spreading length of the beam, and for the on-axis location of the particle, we consider $z_0 = 0$ and $\rho_n = (\frac{n+1/2}{2\pi})\lambda_0$; here $\lambda_0 = \frac{\lambda}{n^w}$. Mie scattering coefficients (MSCs) for the particle are [31,32]: $a_n = (\frac{\psi_n(\alpha)\psi_n'(M\alpha) - M\psi_n'(\alpha)\psi_n(M\alpha)}{\xi_n(\alpha)\psi_n'(M\alpha) - M\xi_n'(\alpha)\psi_n(M\alpha)})$ and $b_n = (\frac{M\psi_n(\alpha)\psi_n'(M\alpha) - \psi_n'(\alpha)\psi_n(M\alpha)}{M\xi_n(\alpha)\psi_n'(M\alpha) - \xi_n'(\alpha)\psi_n(M\alpha)})$, where the variable x is $\alpha = k \times a$; k is the propagation wave vector and a is the radius of the particle. Here, $\psi_n(x)$ and $\xi_n(x)$ are the spherical Bessel functions of positive and negative half-integer order. All parameters used in the simulation are listed in Table I. In the numerical simulation, we have phenomenologically incorporated the optical Kerr effect (OKE), which gives an instantaneous response to high peak power pulses. According to OKE, the relative RI is modifying as $M = \frac{n_0^p}{n_0^w}$ under cw excitation and under pulsed excitation, we use the relative RI as $\frac{n_0^p + n_2^p \times I_{\text{peak}}(r,z)}{n_0^w} = M + 4.44 \times 10^{-17} \times I_{\text{peak}}(r,z)$. The first term is the linear RI of the material while the second term accounts for optical nonlinearity. Note that we have considered only the OKE as optical nonlinearity, which leads to self-focusing, self-phase modulation, etc. The OKE is an instantaneous process that occurs when a strong field interacts with the particle resulting in a change of the relative RI of the material. Higher-order nonlinearity may contribute significantly, as was shown for metallic nanoparticles [34,35]. However, for dielectric nanoparticles, due to higher-order terms, the change occurs in the third digit, which can be safely ignored, and so, we did not consider here any contribution from higher-order nonlinear RIs. A detailed discussion on defining the RI for the particle is given in Sec. B in the Appendix. Here, n_2^p is the second-order nonlinear RI of the particle (which varies depending on the particle material, but in our simulation, we have considered it as constant) and $I_{\text{peak}}(r,z)$ is the intensity of the focused Gaussian beam. The n_2^w is 1000 times less (can be seen from Table I) than n_2^p; therefore, it will not contribute significantly to n_0^w under both cw and pulsed excitation. Hence, it can be ignored. The details of calculating the time-averaged force acting on the particle under pulsed excitation can be seen in Ref. [19].

TABLE I. List of the parameters used in the simulations. RI: refractive index; NRI: nonlinear refractive index.

Parameters used	Symbol	Value/expression
Central wavelength	λ	800 nm
Speed of light	c	3×10^8 m/s
Repetition rate (RR)	RR	76 MHz
Pulse width	τ	120 fs
Peak power	P_{peak}	$\frac{P_{\text{avg}}}{RR \times \tau}$
RI of medium	n_0^w	1.329
Second-order NRI [10]	$n_2^{c/s}$	5.9×10^{-17} m^2/W
Second-order NRI of water [10]	n_2^w	2.7×10^{-20} m^2/W

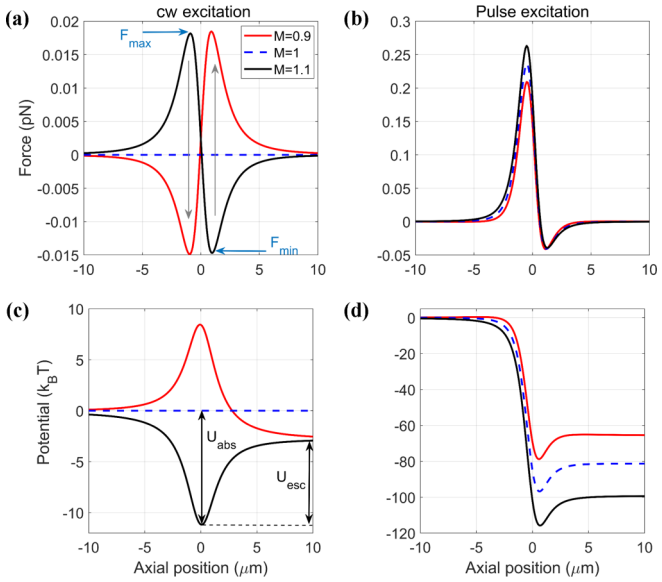

FIG. 1. The plots of trapping force and potential under both cw and pulsed excitations for different M values at 100 mW average power for 40 nm particle size for numerical aperture (NA) = 1.4.

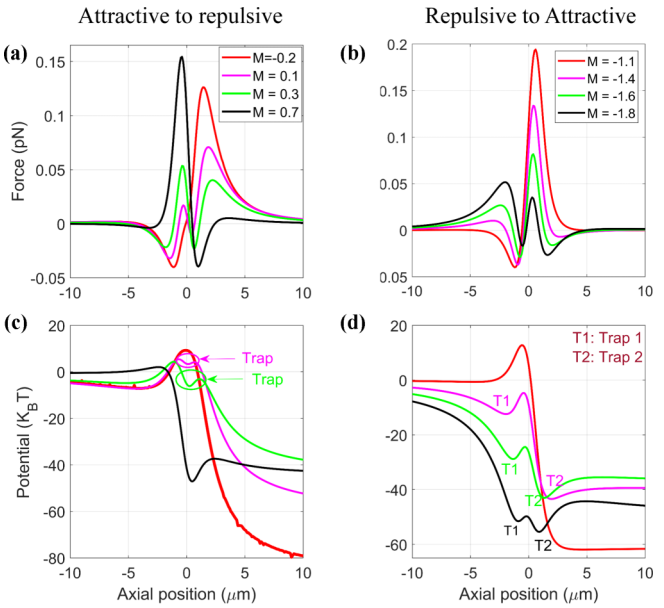

FIG. 2. The plots of trapping force (a,b) and corresponding potential (c,d) at different M values where the transition is occurring from attractive to repulsive or repulsive to attractive under pulsed excitation for 40 nm particle size at 100 mW average power for fixed NA = 1.4.

III. RESULTS AND DISCUSSION

Here, we have assessed the trapping force and potential for both cw and pulsed excitations. Remarkably, we have tested the validity of GLMT using localized approximation and compared the results with dipole approximation ($a \leqslant \frac{\lambda}{20}$; a is the radius of the particle, and λ is the wavelength of the trapping beam) [21]; on that account, we have analyzed the 40 nm particle size separately since 40 nm is limiting for dipole approximation when the trapping beam wavelength is 800 nm.

Figure 1 shows the comparison of force and potential under both cw and pulsed excitation for different M. Here, $F_{\max}$ and $F_{\min}$ represent the maximum and minimum trapping force (marked by arrows); U_{abs} represents the absolute depth of the potential well; and U_{esc}, called the escape potential [19], is the potential barrier along the direction of light propagation. For stable trapping $F_{\max} > 0$ and $F_{\min} < 0$; these are the required conditions. $F_{\max} > 0$ and $F_{\min} < 0$ indicates the attractive force and $F_{\max} < 0$ and $F_{\min} > 0$ indicates that the force is repulsive. Under cw excitation, it can be seen that for $M = 1$, there is no trapping force because the particle's RI is equal to the surrounding medium, which leads to vanishing of the scattering coefficient. When the $M < 1$ particle experiences a repulsive force, it indicates no trapping (as it was known over the decades that a particle having a RI less than the surrounding medium could not be trapped using cw excitation). Yet, under pulsed excitation, if we compare results for $M = 0.9$ and 1, the U_{esc} is greater than $15k_BT$ which indicates stable trapping due to the significant contribution of nonlinear phenomena. For $M > 1$, the U_{esc} is $>10k_BT$, which indicates stable trapping, and it is also evident that the trap is more stable than cw excitation under similar conditions. From these results, we can conjecture that we can trap those nanoparticles under pulsed excitation, which cannot be trapped under cw excitation. For example, we can trap nanoparticles that have RI less than the surrounding medium by taking advantage of nonlinear phenomena. We observe a sharp transition around $M = \pm 1$ from attractive to repulsive force or potential under cw excitation [Figs. 1(a) and 1(c)]. This gradual transition occurs at lower M values under pulsed excitation (Fig. 2). The M value at which transition occurs is different for positive and negative (metamaterials) RI material. In other words, we can say that under cw excitation, the nature of force and potential is symmetric around the origin ($M = 0$); however, no such correlation is observed in pulsed excitation. For $0.1 < M < 0.4$, an indication of trap is there but U_{esc} is not enough to trap the particle stably. We observe a quite interesting feature here: the splitting of the potential well [highlighted and marked in Figs. 2(c) and 2(d)], which allows two nanoparticles to sit side-by-side because after a certain threshold of M both traps have enough U_{esc} to stably trap the nanoparticles. This phenomenon gives more flexibility in manipulating two particles side-by-side without any beam shaping or beam manipulation.

Note that a comparison of U_{abs} (or, equivalently, the maxima and minima of force) should be made if one seeks to quantify the maximum impulsive force on the particle; alternatively, a comparative study of U_{esc} has to be made if the conditions for the most stable trap are to be ascertained. Fig. 3 shows the U_{esc} against M, and quite interestingly, within the range of -10 to 10, four different regimes of the trapping are observed (please note that the regime in which the trap is splitting, we have considered the higher U_{esc} among both the traps for plotting). The process of stabilizing (regimes R1 and R1′), destabilizing (between the regimes R1 and R2 and R1′ and R2′), and stabilizing again (regimes R2 and R2′) is known as "disappearance and reappearance phenomena." The range of M corresponding to each regime can be seen in Table II. The regimes R1 and R1′ are very well known, but regimes

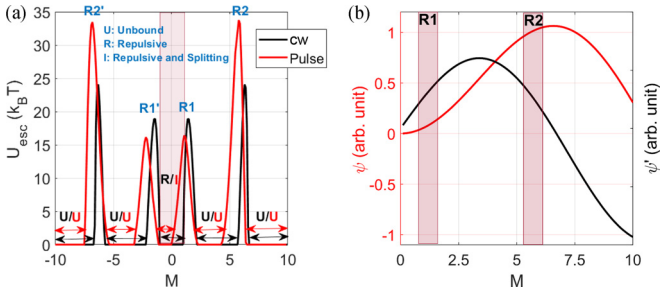

FIG. 3. The plots of (a) $U_{\rm esc}$ against M, and (b) $\psi_1(\alpha)$ and $\psi_1^{'}(\alpha)$ against M values for 40 nm particle size at 100 mW average power under pulsed excitation for fixed NA = 1.4.

R2 and R2′ are unexplored. In regimes R1 and R1′, stable trapping is observed due to a delicate balance between scattering and gradient force but, in between the R1 and R2 (R1′ and R2′) regimes, scattering dominates over the gradient force which results in destabilizing the trap. Hence, researchers have used antireflection coating on top of high-RI particles to be trapped [23,24]. To improve the trapping efficiency in the fall-off regimes (R1, R2, R1′, R2′), antireflection coating can be used because destabilizing the trap in the fall of the regime is implemented by the dominancy of scattering force, and trapping in the R2 and R2′ regimes is observed. Please note that the total force acting along the axial direction is contributed by two major components: (1) MSC and (2) BSC. BSCs are independent of the M, which implies that overall force changes by changing the MSC. Thus, changing the M value changes the MSCs as they are a combination of $\psi_n(\alpha)$, $\psi_n^{'}(\alpha)$, $\xi_n(\alpha)$, $\xi_n^{'}(\alpha)$, $\psi_n(M\alpha)$, and $\psi_n^{'}(M\alpha)$. First four are independent of the M value; thus, MSC changes with changing $\psi_n(M\alpha)$, and $\psi_n^{'}(M\alpha)$. Recently, GLMT using localized approximation was described for dielectric particles, and it was mentioned that for nanoparticles, the first ($n = 1$) term of a_n and b_n contributes significantly to the total force [22], which implies that $\psi_1(M\alpha)$, and $\psi_1^{'}(M\alpha)$ will have the major contribution in total force. Fig. 3(b) shows the plot of $\psi_1(M\alpha)$, and $\psi_1^{'}(M\alpha)$ against M; it can be seen that both factors are increasing in the first regime, but in the second regime, one is decreasing significantly, while the other is increasing. As a result, the combination of both of them will lead to an equal contribution of MSC in the total force in both regimes which is why we can confirm the two different regimes of trapping. Please note that we plotted positive M only, but this behavior is similar for negative M. From the discussion, we can conjecture that there might be many other different regimes of trapping which exist as we go towards a higher M. This happens because Bessel functions are oscillatory, so the same pattern might be repeated in the next cycle, which gives a stable trap indicating that we do not need antireflection coating for all high-RI particles. Comparing cw and pulsed excitation [Fig. 3(a)] shows that both have advantages and disadvantages depending on the relative RI values. For example, at $M = 1.1$, pulse excitation gives the most stable trap while cw excitation shows the particle can trap, but $U_{\rm esc}$ is less than 10 k_BT. That being the case, the particle will leave the trap soon, suggesting that pulsed excitation will improve trapping efficiency more than cw excitation. Furthermore, at $M = 1.4$, cw excitation gives the most stable trap. The pulsed excitation, on the other hand, has less trapping efficiency than cw excitation. One significant advantage of pulsed over cw excitation which cannot be ignored is that trapping a particle with average RI less than the surrounding medium ($0.1 < M < 1$; highlighted rectangle in Fig. 3(a)) cannot be trapped under cw excitation. To get stable trapping of such nanoparticles, we have to take advantage of nonlinear effects. Apart from that, it is evident that in regimes R2 and R2′, pulsed excitation gives overall better trapping efficiency than cw excitation.

Figures 4(a) and 4(b) represent the trapping $F_{\rm max}$ and $F_{\rm min}$ against the M. Please note that the gray arrow in Fig. 1 represents the direction of force $F_{\rm max}$ and $F_{\rm min}$ when we lower M. After a certain value, this trend will be reversed. Consequently, under cw excitation, for $-1 < M < 1$, as we move towards lower M, $F_{\rm max}$ decreases and becomes negative, and after a certain M, it increases again and becomes positive. Similar phenomena occur for the minima, but when the maxima are moving towards negative force values, the minima will move towards the positive force value, and after a threshold, they again decrease and eventually get negative at $M < -1.1$ and $M > 1.1$. At $M = 1$, $F_{\rm max}$ and $F_{\rm min}$ are both zero, evidencing no force acts on the particle (marked points A and B in Fig. 4). However, we observe an exception for the 50 nm particle size, $-0.3 < M < 0.3$, where $F_{\rm max} > 0$ and $F_{\rm min} > 0$, showing no equilibrium point exists, making the

TABLE II. Lists the different regimes M values for trapping events.

Laser type	Attractive to repulsive regime[a]	Repulsive regime	Repulsive to attractive regime[a]	Trapping regime	Most stable trap[a]	Unbound regime
cw	The sudden change at $M = \pm 1$; no trap splitting is observed. Repulsive regime $-1 < M < 1$			$-6.6 < M < -5.8$ $-2.1 < M < -1.1$ $1.1 < M < 2.1$ $5.8 < M < 6.6$	$M = \pm 1.5$ $M = \pm 6.4$	$M < -6.6$ $-5.8 < M < -2.1$ $2.1 < M < 5.8$ $M > 6.6$
Pulsed	$-2.1 < M < -1.1$	$-1.1 < M < -0.1$	$0.1 < M < 0.8$	$-6.7 < M < -6.2$ $-3.1 < M \leqslant -2.1$ $0.8 < M < 1.8$ $5.2 < M < 6.3$	$M = -6.8$ $M = -2.2$ $M = 1.1$ $M = 5.8$	$M < -6.7$ $-6.2 < M < -3.1$ $1.8 < M < 5.2$ $M > 6.3$

[a]Please note that repulsive to attractive and attractive to repulsive is not a sudden transformation under pulsed excitation. Therefore, potential changes gradually pass through the splitting of the potential well.

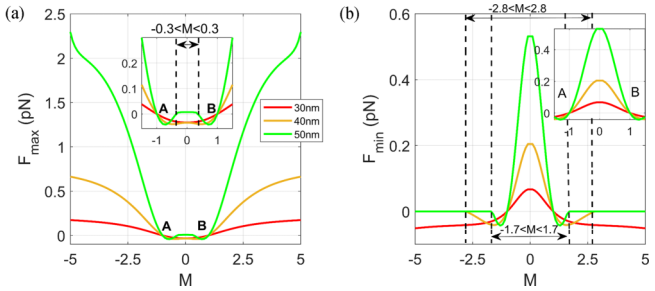

FIG. 4. (a) Maximum force (shown by an arrow in Fig. 1) and (b) minimum force (shown by an arrow in Fig. 1) against M under cw excitation for different particle sizes at 100 mW average power for fixed NA = 1.4.

potential unbound. From the $F_{\max}$ and $F_{\min}$ curves, we can quickly determine which limit allows trapping and which does not. However, it is very difficult to determine which regime would give stable trapping. For example, according to Fig. 4, we can get trapping at $M = 2.7$ for a 40 nm particle size at 100 mW average power. However, according to Fig. 3 at $M = 2.7$, trapping is not stable because $U_{\text{esc}} < 10k_BT$. The widely accepted rule of thumb says if the well depth is more than $10k_BT$, the trap is stable, allowing the U_{esc} curve to give a clear idea of stable ($U_{\text{esc}} > 10k_BT$), unstable ($U_{\text{esc}} < 10k_BT$), and unbound ($U_{\text{esc}} = 0\ k_BT$) trapping. From this, we conclude that to get better trapping information, we should analyze the U_{esc} instead of $F_{\max}$ and $F_{\min}$. Comparision under cw and pulsed excitation is easier for U_{esc} instead of $F_{\max}$ and $F_{\min}$ due to which under pulsed excitation, we are mostly focusing on U_{esc} analysis, and hereafter, we discuss everything in terms of U_{esc}. Under cw excitation [Figs. 3(a) and 6 in the Appendix], U_{esc} also tells us which can be trapped more efficiently under specific conditions. The M value corresponding to maximum U_{esc} is the most stable trap. Most of the researchers mostly report in terms of the trap stiffness; in spite of that, if we calculate the trap stiffness using harmonic approximation, then the trap stiffness at $M = \pm 1.4$ is $\kappa_{\text{stiffness}} \approx 0.11$ pN/μm and $M = \pm 1.8$ is $\kappa_{\text{stiffness}} \approx 0.2$ pN/μm. According to this trap stiffness value, a higher RI gives better trapping stability. Nevertheless, at $M = \pm 1.4$, $U_{\text{esc}} \approx 20k_BT$ and at $M = \pm 1.8$, $U_{\text{esc}} \approx 12\ k_BT$, conveying trap stiffness has decreased by 60%, but according to trap stiffness values, trap stability is increased by approximately 80%. After analyzing the force and potential, we conclude that U_{esc} results are correct, implying that U_{esc} gives more reliable results to determine trapping stability. From this discussion, we can say that the trap is anharmonic due to the significant contribution of scattering force over gradient force. Calculating trap stability using harmonic approximation leads to misleading results.

As we go down in particle size, there is no significant difference in trapping efficiency under both cw and pulse excitations (Fig. 6 in the Appendix). The advantage of using pulse excitation over cw excitation is consistent for nanoparticles having a RI less than the surrounding medium (or $M<1$). Moreover, as we go towards higher particle size, it indicates that cw excitation gives better trap stiffness than pulse excitation. However, when we talk about 50 nm particle size, there is a question of the validity of GLMT using localized approximation because researchers have shown experimentally that the trapping of germanium nanoparticles [36] has a RI around 4.0. According to Fig. 6(b), germanium nanoparticles cannot be trapped whereas the researchers reported the trapping of smaller nanoparticles with higher RI, which agrees with the theoretical results [37]. Hence, we can conclude that the GLMT using localized approximation is not valid for any arbitrary size particle. This theory is valid only for dipole approximation.

Further, we explore the change in trapping efficiency with average power for different particle sizes because changing average power and particle size changes the limiting M value for different regimes. Under cw excitation, power is directly proportional to the force due to which the increasing average power will increase the order of magnitude whereas the nature of the force and potential curve remains the same, which implies that the limits of M for different regimes remain the same for fixed particle size. In addition, there is no change in the repulsive regime under cw excitation, and no splitting in the potential well is observed. In contrast, under pulsed excitation, forces and potentials are nonlinearly dependent on the average power because the relative RI is power dependent. Consequently, the limits of M are changing with changing average power and particle size. Also, the splitting of the potential well is present, but the limit of M for the splitting regime changes with average power and particle size as we move towards higher power and larger particle sizes, and the M limit for distinct trapping events shifts towards a lower M attributed to the increasing contribution of the nonlinear effect. A detailed analysis on the limits of M is listed in Table III.

Later, we observed Fano resonance at different M for fixed NA and vice versa. Increased power increases the magnitude of the force under cw excitation, but the nature of the force curve does not change due to the linear dependence on the average power. Under pulsed excitation, the magnitude and nature of the force curve change drastically with a slight change in the power and M value, as shown in Fig. 5. Please note that for small M, the Fano resonance process starts appearing at high average power [Fig. 5(a)] and for large M, Fano resonance appears at low average power [Fig. 5(b)]. At 200 mW average power, Fano resonance starts contributing to the total force, which is evident by a sharpness in the force curve at $F_{\max}$. As we move from 200 to 250 mW average power, for $M = 5$, the force experienced by the particle is 30 times higher than the force experienced by the particle at 200 mW average power. MSCs are responsible for these oscillations or spikes [22], and this phenomenon is known as Fano resonance. The interference between the scattering amplitude of resonance (discrete level transition) and the background transition causes Fano resonance to emerge in any media [38–44]. It can be understood in terms of excitation of the anapole mode of the particle, which is associated with Fano resonance [40]. The nonradiative anapole mode arises from the destructive interference of electric and toroidal dipoles, which improves scattering efficiency. Because of the significantly increased scattering force, the particle with a much higher RI than the surrounding medium cannot be trapped. As a result, Fano resonance introduces the idea of NOSF (negative optical scattering force) [42], which helps in the

TABLE III. Lists the different regimes M values for trapping events for different particle sizes and average power under both cw and pulsed excitations. Please note that all the details in this table are between the limit $-5 < M < 5$ for trapping events (such as repulsive, attractive, bound, unbound).

Particle size	Laser type	Power (mW)	Attractive to repulsive	Repulsive	Repulsive to attractive	Trapping regime	Most stable trap and beyond	Fano resonance starting point	Unbound regime
30 nm	cw	Independent	The sudden change at $M = \pm 1$; no trap splitting is observed. Repulsive regime $-1 < M < 1$			$-5 \leqslant M \leqslant -1$ $+1 \leqslant M \leqslant +5$	Beyond $M = \pm 5$ (around ± 8.8)	No Fano-resonance	—
	Pulse	50	$-1.6 \leqslant M \leqslant -1.1$	$-1 \leqslant M \leqslant 0.4$	$0.4 \leqslant M \leqslant 0.9$	$-5 \leqslant M \leqslant -1.6$ $M \geqslant 1$		$M = 9.2$	—
		100	$-2 \leqslant M \leqslant -1.2$	$-1.1 \leqslant M \leqslant 0.1$	$0.2 \leqslant M \leqslant 0.8$	$-5 \leqslant M \leqslant -2.1$ $0.9 \leqslant M \leqslant 5$		$M = 8.8$	—
		200	$-3.1 \leqslant M \leqslant -1.2$	$-1.1 \leqslant M \leqslant -1.0$	$-0.9 \leqslant M \leqslant 0.8$	$-5 \leqslant M \leqslant -3.2$ $0.9 \leqslant M \leqslant 5$	Beyond $M = \pm 5$	$M = 8.0$	—
		300	$-4.1 \leqslant M \leqslant 0.7$ (trap splitting is prominent, no evidence of repulsive force)			$-5 \leqslant M \leqslant -4.2$ $0.8 \leqslant M \leqslant 5.0$		$M = 7.0$	—
		400	$-5 \leqslant M \leqslant 0.7$ (trap splitting is prominent, no evidence of repulsive force)			$0.8 \leqslant M \leqslant 5.0$		$M = 5.5$	—
		500	$-5 \leqslant M \leqslant 0.8$ (trap splitting is prominent, no evidence of repulsive force)			$0.9 \leqslant M \leqslant 5.0$	$M = 4.6$	$M = 3.9$	—
40 nm	cw	Independent	The sudden change at $M = \pm 1$; no trap splitting is observed. Repulsive regime $-1 < M < 1$			$-2.1 < M < -1.1$ $1.1 < M < 2.1$	$M = \pm 1.5$	No Fano-resonance	$M < -2.1$ $M > 2.1$
	Pulse	50	$-1.5 \leqslant M \leqslant -1$	$-1 \leqslant M \leqslant 0.4$	$0.5 \leqslant M \leqslant 0.9$	$-3 \leqslant M \leqslant -1.6$ $1 \leqslant M \leqslant 2.5$ $M \geqslant 4.6$	$M = -1.6$ $M = 1$		$M \leqslant -3.1$ $2.5 \leqslant M \leqslant 4.5$
		100	$-2.1 < M < -1.1$	$-1.1 < M < -0.1$	$0.1 < M < 0.8$	$-3.1 < M \leqslant -2.1$ $0.8 < M < 1.8$	$M = -2.2$ $M = 1.1$	$M = 9.5$	$M < -3.1$ $M > 1.8$
		200	$-3.3 \leqslant M \leqslant -1.3$	$-1.2 \leqslant M \leqslant -1.1$	$-1 \leqslant M \leqslant 0.8$	$-3.9 \leqslant M \leqslant -3.3$ $0.9 \leqslant M \leqslant 1.8$ $3.7 \leqslant M$	$M = -3.3$ $M = 0.9$ $M>5$ (beyond range)	$M = 4.8$	$-5 \leqslant M \leqslant 4$ $1.9 \leqslant M \leqslant 3.6$
		300	$-4.2 \leqslant M \leqslant 0.7$ (trap splitting is prominent, no evidence of repulsive force)			$-4.7 \leqslant M \leqslant -4.3$ $0.8 \leqslant M \leqslant 1.3$ $3.1 \leqslant M$	$M = -4.3$ $M = 0.8$ $M = 4.5$	$M = 3.5$	$-5 \leqslant M \leqslant -4.8$ $1.4 \leqslant M \leqslant 3.0$
		400	$-5 \leqslant M \leqslant 0.5$ (trap splitting is prominent, no evidence of repulsive force)			$0.5 \leqslant M \leqslant 1.3$ $2.3 \leqslant M$	$M = 0.5$ $M = 4.1$	$M = 2.3$	$1.4 \leqslant M \leqslant 2.2$
		500	$-5 \leqslant M \leqslant 0.2$ (trap splitting is prominent, no evidence of repulsive force)			$0.3 \leqslant M \leqslant 1.2$ $1.5 \leqslant M$	$M = 0.3$ $M = 3.0$	$M = 1.1$	$1.3 \leqslant M \leqslant 1.4$

[a]Please note that repulsive to attractive and attractive to repulsive is not a sudden transformation under pulsed excitation. Therefore, potential changes gradually pass through the splitting of the potential well.

[b]Please note that the Fano resonance phenomena are present even beyond $M = 5$.

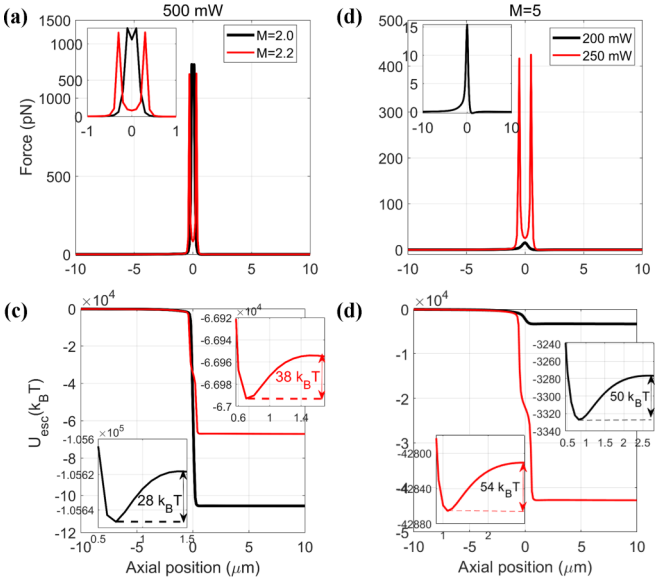

FIG. 5. Plots of trapping force (a), (b) and corresponding potential (c), (d) against the axial position under pulsed excitation for 40 nm particle size and NA = 1.4. Left panel: for different M and fixed power. Right panel: different power and fixed M.

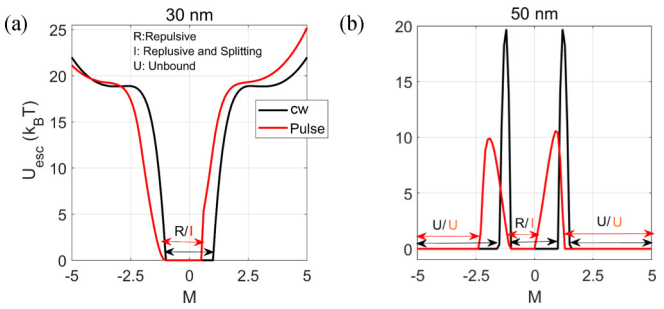

FIG. 6. The plot of U_{esc} against M (relative refractive index) for (a) 30 nm and (b) 50 nm under both cw and pulsed excitation at 100 mW average power for fixed NA = 1.4. Trapping stability is classified into different regimes based on the values of the relative refractive index and the corresponding escape potential, such as R representing the repulsive regime, where the particle experiences the repulsive force and cannot be trapped, I representing the repulsive and splitting regime, where the particle can be trapped within splitting regime but only for a short period of time, and U representing the unbound regime, where the particle will get trapped and immediately leave the trap.

trapping of such nanoparticles. Clear evidence can be seen from the trapping potential [Figs. 5(c) and 5(d)], where at fixed average power, increasing M value increases the U_{esc} which indicates that the trap is moving towards stability. Even so, according to the rule of thumb, U_{esc} is enough to stably trap a particle. Similarly, for fixed $M = 5$, increasing average power increases the U_{esc}. Interestingly, the most stable trap lies in the Fano resonance regime, which implies that Fano resonance helps nanoparticles to trap better. In Table III, all the highlighted values of the most stable point for a 40 nm particle are due to Fano resonance. Similar behavior is observed for metamaterials as well. Hence, depending on the value of M, the nature of forces and potentials are broadly categorized into four regimes: *splitting*, *repulsive*, *attractive*, and *unbound*. In addition to this, we observed the Fano resonance phenomena under pulsed excitation due to the significant contribution of nonlinear phenomena that help us trap high-RI nanoparticles using NOSF.

IV. CONCLUSION

In summary, using generalized Lorentz-Mie theory, we have theoretically shown how optical nonlinearity in laser trapping of dielectric nanoparticles leads to the emergence of novel phenomena that may be harnessed for controlled nanoscale optical manipulation with far-reaching technical applications.

The authors declare no conflicts of interest.

APPENDIX

Theory

A. Approximation in numerical simulations

Metamaterials have a large dispersion of permittivity, and it depends on many factors such as shape, size, wavelength of incident beam, etc. The metamaterial dispersion effects are more prominent when wavelength ($\lambda > 1.2\ \mu$m) or frequency is in GHz [45–50]. The trapping wavelength we chose here is 800 nm and this effect can be ignored because the change in the electric and magnetic permeability is negligible below $\lambda < 1.5\ \mu$m (see Figs. 3 and 4 in Ref. [45], and Fig. 1(b) in Ref. [46]). Figure 1 of Ref. [49] indicates that this effect for imaginary refractive index is almost negligible for 800 nm; however, it is significant near resonance *and* in the deep IR wavelength regime.

B. Defining refractive index

Please note that in this paper, we have revisited the problem for dielectric particles or particles having higher real refractive index and negligible imaginary part of the refractive index such as titanium dioxide, germanium, ZnO, etc. For metal particles (which have complex refractive index), we also need to account for the interband transitions which are not present in the dielectric particles. Metamaterials are known to have negligible imaginary refractive index around 800 nm wavelength [51]. Hence, our simulations are valid for a wide range of particles where absorption is not a dominating factor. Apart from that, this calculation has been performed for considering the application of optical tweezers for bioconjugated applications. For the bioconjugated experiment, absorption can lead to give significant thermal effect. Hence, those particles cannot be used.

C. Dielectric and metallic particles

The results for dielectrics hold equally for nanoparticles as well. However, we have another extra force named the absorption force acting on the particle for metallic nanoparticles calculation. The direction of absorption force is the same as the scattering force which leads these particles to destabilize faster than the dielectric nanoparticles. A detailed discussion can be seen in Refs. [19,34,35].

[1] A. Ashkin, *Optical Trapping and Manipulation of Neutral Particles Using Lasers: A Reprint Volume with Commentaries* (World Scientific, Singapore, 2006).

[2] A. Ashkin, J. M. Dziedzic, J. E. Bjorkholm, and S. Chu, Observation of a single-beam gradient force optical trap for dielectric particles, Opt. Lett. **11**, 288 (1986).

[3] A. E. Larsen and D. G. Grier, Like-charge attraction in metastable colloidal crystallites, Nature (London) **385**, 230 (1997). v.

[4] M. P. MacDonald, G. C. Spalding, and K. Dholakia, Microfluidic sorting in an optical lattice, Nature (London) **426**, 421 (2003).

[5] D. T. Chiu and R. N. Zare, Biased diffusion, optical trapping, and manipulation of single molecules in solution, J. Am. Chem. Soc. **118**, 6512 (1996).

[6] P. M. Hansen, V. K. Bhatia, N. Harrit, and L. Oddershede, Expanding the optical trapping range of gold nanoparticles, Nano Lett. **5**, 1937 (2005).

[7] S. M. Block, L. S. B. Goldstein, and B. J. Schnapp, Bead movement by single kinesin molecules studied with optical tweezers, Nature (London) **348**, 348 (1990).

[8] D. E. Smith, S. J. Tans, S. B. Smith, S. Grimes, D. L. Anderson, and C. Bustamante, The bacteriophage $\phi 29$ portal motor can package DNA against a large internal force, Nature (London) **413**, 748 (2001).

[9] B. Agate, C. T. A. Brown, W. Sibbett, and K. Dholakia, Femtosecond optical tweezers for *in-situ* control of two-photon fluorescence, Opt. Express **12**, 3011 (2004).

[10] L. Pan, A. Ishikawa, and N. Tamai, Detection of optical trapping of cdte quantum dots by two-photon-induced luminescence, Phys. Rev. B **75**, 161305(R) (2007).

[11] A. K. De, D. Roy, A. Dutta, and D. Goswami, Stable optical trapping of latex nanoparticles with ultrashort pulsed illumination, Appl. Opt. **48**, G33 (2009).

[12] J. C. Shane, M. Mazilu, W. M. Lee, and K. Dholakia, Effect of pulse temporal shape on optical trapping and impulse transfer using ultrashort pulsed lasers, Opt. Express **18**, 7554 (2010).

[13] A. Usman, W.-Y. Chiang, and H. Masuhara, Optical trapping and polarization-controlled scattering of dielectric spherical nanoparticles by femtosecond laser pulses, J. Photochem. Photobiol. A: Chem. **234**, 83 (2012).

[14] A. Usman, W.-Y. Chiang, and H. Masuhara, Optical trapping of nanoparticles by ultrashort laser pulses, Sci. Prog. **96**, 1 (2013).

[15] W.-Y. Chiang, A. Usman, and H. Masuhara, Femtosecond pulse-width dependent trapping and directional ejection dynamics of dielectric nanoparticles, J. Phys. Chem. C **117**, 19182 (2013).

[16] W.-Y. Chiang, T. Okuhata, A. Usman, N. Tamai, and H. Masuhara, Efficient optical trapping of cdte quantum dots by femtosecond laser pulses, J. Phys. Chem. B **118**, 14010 (2014).

[17] T.-H. Liu, W.-Y. Chiang, A. Usman, and H. Masuhara, Optical trapping dynamics of a single polystyrene sphere: Continuous wave versus femtosecond lasers, J. Phys. Chem. C **120**, 2392 (2016).

[18] A. Kittiravechote, A. Usman, H. Masuhara, and I. Liau, Enhanced optical confinement of dielectric nanoparticles by two-photon resonance transition, RSC Adv. **7**, 42606 (2017).

[19] A. Devi and A. K. De, Theoretical investigation on nonlinear optical effects in laser trapping of dielectric nanoparticles with ultrafast pulsed excitation, Opt. Express **24**, 21485 (2016).

[20] A. Devi, S. Yadav, and A. K. De, Dynamics of a dielectric microsphere inside a nonlinear laser trap, Appl. Phys. Lett. **117**, 161102 (2020).

[21] A. Devi and A. K. De, Generalized description of the nonlinear optical force in laser trapping of dielectric nanoparticles, Phys. Rev. Research **2**, 043378 (2020).

[22] A. Devi and A. K. De, Generalized lorenz-mie theory for the reversal of optical force in a nonlinear laser trap, Phys. Rev. A **102**, 023509 (2020).

[23] Y. Hu, T. A. Nieminen, N. R. Heckenberg, and H. Rubinsztein-Dunlop, Antireflection coating for improved optical trapping, J. Appl. Phys. **103**, 093119 (2008).

[24] N. Wang, X. Li, J. Chen, Z. Lin, and J. Ng, Gradient and scattering forces of anti-reflection-coated spheres in an aplanatic beam, Sci. Rep. **8**, 17423 (2018).

[25] S. Anantha Ramakrishna and T. M. Grzegorczyk, *Physics and Applications of Negative Refractive Index Materials* (CRC Press, Boca Raton, FL and SPIE Press, Bellingham, WA, 2008).

[26] G. V. Eleftheriades and K. G. Balmain, *Negative-Refraction Metamaterials: Fundamental Principles and Applications* (John Wiley & Sons, New York, 2005).

[27] V. I. Slyusar, Metamaterials on antenna solutions, in *Proceedings of 7th International Conference on Antenna Theory and Techniques, ICATT'09* (2009).

[28] T. Tang, Surface modes in an asymmetrical waveguide with dispersive single-negative metamaterial, Optik **124**, 6493 (2013).

[29] S. A. Tretyakov and S. I. Maslovski, Veselago materials: what is possible and impossible about the dispersion of the constitutive parameters, IEEE Antennas Propag. Mag. **49**, 37 (2007).

[30] I. S. Nefedov and S. A. Tretyakov, Photonic band gap structure containing metamaterial with negative permittivity and permeability, Phys. Rev. E **66**, 036611 (2002).

[31] G. Gouesbet and G. Grehan, *Generalized Lorentz-Mie theory* (Springer, Berlin, 2011).

[32] G. Gouesbet, G. Grehan, and B. Maheu, Light scattering from a sphere arbitrarily located in a gaussian beam, using a bromwich formulation, J. Opt. Soc. Am. A **5**, 1427 (1988).

[33] G. Gouesbet, G. Grehan, and B. Maheu, Localized interpretation to compute all the coefficients g_{nm} in the generalized lorentz-mie theory, J. Opt. Soc. Am. A **7**, 998 (1990).

[34] A. Devi, S. S. Nair, and A. K. De, Disappearance and reappearance of an optical trap for silver nanoparticles under femtosecond pulsed excitation: A theoretical investigation, Europhys. Lett. **126**, 28002 (2019).

[35] A. Devi, S. Yadav, and A. K. De, Synergistic effect of fano resonance and optical nonlinearity in laser trapping of silver nanoparticles, Phys. Rev. A **102**, 043511 (2020).

[36] S. Sudhakar, M. K. Abdosamadi, T. J. Jachowski, M. Bugiel, A. Jannasch, and E. Schäffer, Germanium nanospheres for ultraresolution picotensiometry of kinesin motors, Science **371**, 6530 (2021).

[37] P. Purohit, A. Samadi, P. M. Bendix, J. J. Laserna, and L. B. Oddershede, Optical trapping reveals differences in dielectric and optical properties of copper nanoparticles compared to their oxides and ferrites, Sci. Rep. **10**, 1198 (2020).

[38] M. V. Rybin, K. B. Samusev, I. S. Sinev, G. Semouchin, E. Semouchkina, Y. S. Kivshar, and M. F. Limonov, Mie scattering as a cascade of fano resonances, Opt. Express **21**, 30107 (2013).

[39] X. Kong and G. Xiao, Fano resonances in core-shell particles with high permittivity covers, in *Progress in Electromagnetic Research Symposium* (IEEE, New York, 2016), pp. 1715–1719.

[40] B. Lukyanchuk, R. Paniagua-Domínguez, A. I. Kuznetsov, A. E. Miroshnichenko, and Y. S. Kivshar, Suppression of scattering for small dielectric particles: Anapole mode and invisibility, Philos. Trans. R. Soc. A **375**, 20160069 (2017).

[41] M. Kroner, A. O. Govorov, S. Remi, B. Biedermann, S. Seidl, A. Badolato, P. M. Petroff, R. Barbour, W. Zhang, B. D. Gerardot, R. J. Warburton, and K. Karrai, The nonlinear fano effect, Nature (London) **451**, 311 (2008).

[42] H. Chen, S. Liu, J. Zi, and Z. Lin, Fano resonance-induced negative optical scattering force on plasmonic nanoparticles, ACS Nano **9**, 1926 (2015).

[43] M. I. Tribelsky, S. Flach, A. E. Miroshnichenko, A. V. Gorbach, and Y. S. Kivshar, Light Scattering by a Finite Obstacle and Fano Resonances, Phys. Rev. Lett. **100**, 043903 (2008).

[44] B. Luk'yanchuk, N. I. Zheludev, S. A. Maier, N. J. Halas, P. Nordlander, H. Giessen, and C. T. Chong, The fano resonance in plasmonic nanostructures and metamaterials, Nat. Mater. **9**, 707 (2010).

[45] J. Jung, H. Park, J. Park, T. Chang, and J. Shin, Broadband metamaterials and metasurfaces: A review from the perspectives of materials and devices, Nanophotonics **9**, 3165 (2020).

[46] Y. Zhou, Z. Qin, Z. Liang, D. Meng, H. Xu, D. R. Smith, and Y. Liu, Ultra-broadband metamaterial absorbers from long to very long infrared regime, Light: Sci. Appl. **10**, 138 (2021).

[47] Z. H. Jiang, S. Yun, L. Lin, J. A. Bossard, D. H. Werner, and T. S. Mayer, Tailoring dispersion for broadband low-loss optical metamaterials using deep-subwavelength inclusions, Sci. Rep. **3**, 1571 (2013).

[48] P. Wang, N. Chen, C. Tang, J. Chen, F. Liu, S. Sheng, B. Yan, and C. Sui, Engineering the complex-valued constitutive parameters of metamaterials for perfect absorption, Nanoscale Res. Lett. **12**, 276 (2017).

[49] Z. Y. Zhou, D. S. Ding, B. S. Shi, X. B. Zou, and G. C. Guo, Characterizing dispersion and absorption parameters of metamaterial using entangled photons, Phys. Rev. A, **85**, 023841 (2012).

[50] S. J. Palmer, X. Xiao, N. Pazos-Perez, L. Guerrini, M. A. Correa-Duarte, S. A. Maier, R. V. Craster, R. A. Alvarez-Puebla, and V. Giannini, Extraordinarily transparent compact metallic metamaterials, Nat. Commun. **10**, 2118 (2019).

[51] B. T. Schwartz and R. Piestun, Total external reflection from metamaterials with ultralow refractive index, J. Opt. Soc. Am. B **20**, 2448 (2003).